



Open Archive TOULOUSE Archive Ouverte (OATAO)

OATAO is an open access repository that collects the work of Toulouse researchers and makes it freely available over the web where possible.

This is an author-deposited version published in : <http://oatao.univ-toulouse.fr/>
Eprints ID : 14402

To link to this article : doi: 10.1017/jfm.2015.559
URL : <http://dx.doi.org/10.1017/jfm.2015.559>

<p>To cite this version : Thual, Olivier and Lacaze, Laurent and Mouzouri, Miloud and Boutkhamouine, Brahim Critical slope for laminar transcritical shallow-water flows. (2015) Journal of Fluid Mechanics, vol. 783. PP. 1-11. ISSN 0022-1120</p>
--

Any correspondence concerning this service should be sent to the repository administrator: staff-oatao@listes-diff.inp-toulouse.fr

Critical slope for laminar transcritical shallow-water flows

O. Thual^{1,2,†}, L. Lacaze^{1,2}, M. Mouzouri^{1,2} and B. Boutkhamouine^{1,2}

¹Université de Toulouse; INPT, UPS; IMFT, Allée Camille Soula, F-31400 Toulouse, France

²CNRS; IMFT; F-31400 Toulouse, France

Backwater curves denote the depth profiles of steady flows in a shallow open channel. The classification of these curves for turbulent regimes is commonly used in hydraulics. When the bottom slope I is increased, they can describe the transition from fluvial to torrential regimes. In the case of an infinitely wide channel, we show that laminar flows have the same critical height h_c as that in the turbulent case. This feature is due to the existence of surface slope singularities associated to plug-like velocity profiles with vanishing boundary-layer thickness. We also provide the expression of the critical surface slope as a function of the bottom curvature at the critical location. These results validate a similarity model to approximate the asymptotic Navier–Stokes equations for small slopes I with Reynolds number Re such that ReI is of order 1.

Key words: interfacial flows (free surface), low-Reynolds-number flows, thin films

1. Introduction

Shallow-flow modelling usually eliminates one or two spatial dimensions by considering average properties over the depth of a thin fluid layer. This modelling approach is current in hydraulics (Chow 1959), dealing with turbulent open-channel flows. In this context, backwater curves denote 1D steady depth profiles $h(x)$ and obey the backwater equation $(1 - Fr)h' = I - J$ where Fr is a Froude number, I is the bottom slope and J is the lineic head loss due to bottom friction. When $I > 0$ is constant, the relative values of the critical height h_c , such that $Fr = 1$, and the normal height h_n , such that $I = J$, lead to three M -curve types in the weak slope regime $h_c < h_n$ and to three S -curve types in the strong slope regime $h_n < h_c$. When $I(x)$ varies with space, transitions between the fluvial ($Fr < 1$) and the torrential ($Fr > 1$) regimes can occur through hydraulic jumps or transcritical transition (e.g. Bukreev, Gusev & Lyapidevskii 2002 or Zerihun & Fenton 2006). These backwater curves can

† Email address for correspondence: thual@imft.fr

be viewed as steady solutions of the Saint-Venant equations (de Saint-Venant 1871), also called the shallow-water equations.

The laminar flows of thin viscous liquid layers are also modelled by shallow-flow equations. Benney (1966) and Shkadov (1967) derived such models by retaining only a parabolic velocity profile in a Galerkin approximation of the 2D vertical Navier–Stokes equations and justified it by the good agreement with the experiments of Kapitsa & Kapitsa (1949). Numerous subsequent works have proposed asymptotic expansion leading to a 1D partial differential equation for the depth $h(x, t)$ and the lineic discharge flux $q(x, t)$, often taking into account the effect of surface tension and considering various bottom slopes (Lin 1969; Gjevik 1970; Nakaya 1975; Pumir, Manneville & Pomeau 1983; Alekseenko, Nakoryakov & Pokusaev 1985; Roberts 1996; Oron, Davis & Bankoff 1997; Ruyer-Quil & Manneville 1998, 2000, 2005; Nguyen & Balakotaiah 2000; Shkadov & Sisoev 2004; Boutounet *et al.* 2008; Sadiq & Usha 2008; Fernández-Nieto, Noble & Vila 2010; Samanta, Ruyer-Quil & Goyeau 2011; Noble & Vila 2013; Chakraborty *et al.* 2014, ...). Starting with the so-called ‘boundary-layer equation’, similar to Prandtl’s equations (Schlichting 1955), the difficulty of these modelling approaches lies in the information required about the velocity profile in the integration direction. Most works suggest fixed shapes such as the parabolic one in the laminar cases. More elaborate approaches, such as the weighted-residual method of Ruyer-Quil & Manneville (1998), are based on well suited Galerkin approximation functions that minimize the number of resulting equations. Following a different approach, we present an approximation method that leads to a single backwater equation associated with similarity solutions for the velocity profiles.

Here, we consider laminar flows of Newtonian fluids with negligible surface tension effects in the presence of a small and slowly varying bottom slope such that the product $\Gamma = ReI$ of the slope I and the Reynolds number Re is of order one, while I is small. For instance, the case $I = 0.01$ and $Re = 100$ satisfies this requirement while ensuring that the flow is laminar. As for most asymptotic expansions, this choice aims to balance a maximum of terms in the equations, that is, for the present case, acceleration, pressure, bottom slope and friction in the momentum equations.

Under this asymptotic expansion, we express the steady solution velocities in the form $u = T/h$ and $v = L(dh/dX)/h - \partial M/\partial X$ where T , L and M are functions of $X = x/Re$ and $Y = y/h$, being related through $L = YT$ and $\partial M/\partial Y = T$. This leads to the ‘TLM model’ in which the X dependency of the T profiles is contained in the term $h[(\partial M/\partial X)(\partial T/\partial Y) - (\partial T/\partial X)T]$ that appears to be often small compared to the others. When it is so, the steady flow is described by the similarity model in which T and L no longer depend on X (STL model). Such a similarity assumption for the velocity profiles was introduced by Serre (1953), but the shape of the velocity profiles had to be imposed eventually. Instead of using a Galerkin approximation and averaging over the vertical, as is often done in the literature, our TLM and STL models involve an implicit relation for h and dh/dX through a nonlinear 1D eigenvalue problem, as explained in § 2. These models are then compared to each other in § 3 in the case of transcritical flows.

2. Three shallow-water steady models

2.1. The TLM shallow-water model

We consider an infinitely wide channel whose bottom is defined by the equation $z = Z_f(x)$ where (x, z) are respectively the horizontal and vertical coordinates in the

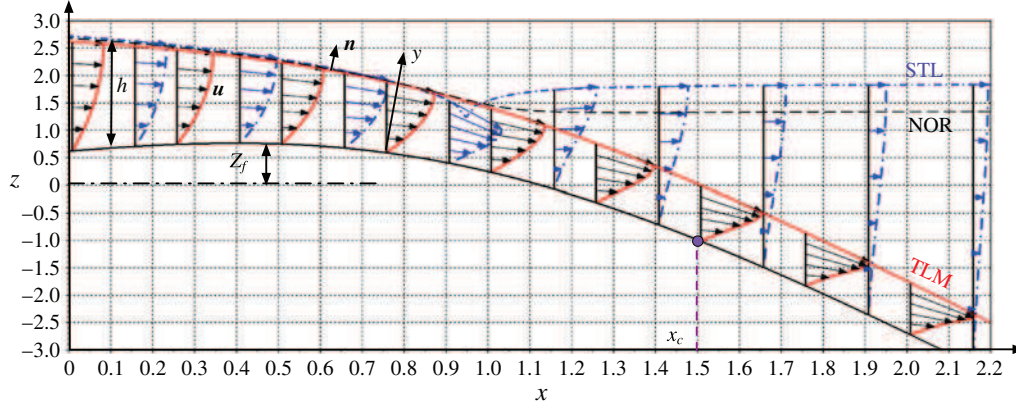


FIGURE 1. 2D flow \mathbf{u} of a layer of depth h over a slowly variable bottom $z = Z_f(x)$. Comparison of three shallow-water steady models for a transcritical flow: TLM in plain red, STL in dash-dotted blue and NOR in dashed black. The TLM backwater curve is critical at $x = x_c$.

presence of gravity g (figure 1). If y denotes the coordinate perpendicular to the bottom at some location, we suppose that the slope $I = -Z_f'(x)$ is small enough to consider that x is also the coordinate in the direction tangential to the bottom. Within this approximation and denoting by φ_x the derivatives $(\partial\varphi/\partial x)(x, y)$ or $\varphi'(x)$ of a quantity φ , the steady 2D incompressible Navier–Stokes equations read

$$\left. \begin{aligned} \tilde{u}_x + \tilde{v}_y &= 0, & \tilde{u}\tilde{u}_x + \tilde{v}\tilde{u}_y &= -\tilde{p}_x + I + Re^{-1}(\tilde{u}_{xx} + \tilde{u}_{yy}), \\ \tilde{u}\tilde{v}_x + \tilde{v}\tilde{v}_y &= -\tilde{p}_y - 1 + Re^{-1}(\tilde{v}_{xx} + \tilde{v}_{yy}), \end{aligned} \right\} \quad (2.1)$$

where the velocities \tilde{u} and \tilde{v} are made non-dimensional by $q^{1/3}g^{1/3}$ and all spatial coordinates by $q^{2/3}g^{-1/3}$, with q denoting the constant lineic discharge flux. The Reynolds number is $Re = q/\nu$ where ν is the kinematic viscosity.

The boundary conditions at the bottom, defined by the equation $y = 0$, are $\tilde{u} = \tilde{v} = 0$. On the free surface, defined by the equation $y = \tilde{h}(x)$, the kinematic and dynamic boundary conditions are respectively $\tilde{u}\tilde{h}_x = \tilde{v}$ and $(\tilde{p} - \tilde{p}_a)\mathbf{n} = 2Re^{-1}\tilde{\mathbf{d}} \cdot \mathbf{n}$ where p_a is the constant atmospheric pressure, \mathbf{n} is the normal to the free surface and $\tilde{\mathbf{d}}$ is the strain rate tensor.

Since the slope I is small, we consider the following asymptotic expansion with $\epsilon \ll 1$:

$$\left. \begin{aligned} \epsilon &= Re^{-1}, & \Gamma &= ReI, & \tilde{h} &= h(\epsilon x) + O(\epsilon), \\ \tilde{u} &= u(\epsilon x, y) + O(\epsilon), & \tilde{v} &= \epsilon v(\epsilon x, y) + O(\epsilon^2), & \tilde{p} &= p(\epsilon x, y) + O(\epsilon), \end{aligned} \right\} \quad (2.2)$$

where Γ , h , v and p are of order one. Since $I = O(\epsilon)$, the coordinate x can be considered to refer to the direction tangential to the bottom. We denote by $X = \epsilon x$ the slow streamwise coordinate. At the leading order of the expansion, one gets the following system for $u(X, y)$, $v(X, y)$ and $h(X)$:

$$u_x + v_y = 0, \quad uu_x + vv_y = -h_x + \Gamma + u_{yy}, \quad (2.3a,b)$$

with $u(X, 0) = v(X, 0) = 0$, $u(X, h)h_X = v(X, h)$ and $u_y(X, h) = 0$ for the boundary conditions, with $\int_0^h u(X, y) dy = 1$ as a constraint to express the constant dimensionless discharge flux. Note that the pressure p is hydrostatic in the framework of this analysis.

We look at solutions of (2.3a,b) with the general form

$$u(X, y) = \frac{1}{h(X)} T \left(X, \frac{y}{h(X)} \right), \quad (2.4)$$

which leads to the ‘TLM model’ for $T(X, Y)$ and $h(X)$:

$$0 = T_{YY} + h^3(\Gamma - h_X) + h_X T^2 + h(M_X T_Y - T_X T), \quad (2.5)$$

where $M(X, Y) = \int_0^Y T(X, Z) dZ$, with $T(X, 0) = T_Y(X, 1) = 0$ and $M(X, 1) = 1$. The vertical velocity reads $v = (h_X/h)L(X, y/h) - M_X$ with $L(X, Y) = YT(X, Y)$.

This equation with its three constraints determines one unknown scalar. If we impose a bathymetry $Z_f(X)$ of slope $\Gamma(X) = -Z_f'(X)$, we can compute $h'(X) = \Sigma$ where Σ is the solution of (2.5) and then integrate to obtain the backwater curve $h(X)$.

2.2. The one-parameter family profiles of the STL model

We denote by ‘STL’ the model obtained by ignoring the h term ($M_X T_Y - T_X T$) in the TLM model. Similarity solutions $u(X, y) = T[y/h(X)]/h(X)$ are thus described by this STL model. Denoting $\Delta = h^3(\Gamma - \Sigma)$, this model reduces to the ordinary differential equation $0 = T'' + \Delta + \Sigma T^2$, subject to the three constraints $T(0) = T'(1) = 0$ and $\int_0^1 T(Y) dY = 1$. We use a finite difference scheme $(N-1)^2(T_{n+1} - 2T_n + T_{n-1})$ for $n = 2, \dots, N-1$ to approximate T'' , where the T_n values are the values of T at N equally distributed points in the interval $Y \in [0, 1]$. The three constraints of (2.5) read $T_1 = T_N - T_{N-1} = 0$ and $\sum_1^N T_n = N$. The function `fsolve` of Scilab (Scilab Enterprises 2012) is used with Σ considered as a control parameter to determine a branch of solutions $\Sigma = \mathcal{S}(\Delta)$. We have checked that the resolution $N = 101$ provided sufficient accuracy for most of the cases presented here.

Part of the branch of solutions $\Sigma = \mathcal{S}(\Delta)$ passing through the linear case $(\Sigma, \Delta) = (0, 3)$ is displayed in figure 2. The corresponding velocity profiles $T_\Delta(Y)$ range from a shear profile for $\Delta = -\infty$ up to a plug-like profile ($T_\infty = 1$ with a boundary layer at $Y = 0$) for $\Delta = \infty$, passing through the parabolic profile $T_3(Y) = (3/2)Y(2 - Y)$ for the linear case.

In order to obtain a synthetic overview of our STL model, we integrate the equation $0 = T'' + \Delta + \Sigma T^2$ over the interval $Y \in [0, 1]$ to obtain

$$[h^3 - \beta(\Delta)]h'(X) = h^3 \Gamma(X) - \alpha(\Delta) \quad \text{with} \quad \Delta = h^3[\Gamma(X) - h'(X)], \quad (2.6)$$

where $\alpha(\Delta) = T'_\Delta(0)$ and $\beta(\Delta) = \int_0^1 T_\Delta^2(Y) dY$ are plotted in figure 3(a). When the velocity profile T_Δ is the parabolic solution T_3 , one recovers the values $\alpha(3) = 3$ and $\beta(3) = 1.2$ that are commonly used for laminar shallow flows. The solutions $\Sigma = h'(X)$ of the implicit (2.6) are displayed in figure 3(b) as functions of h for various values of Γ . For $\Gamma \in [1.82, 3]$, the resulting backwater curves exhibit more complex topologies than the usual one obtained with constant values of α and β .

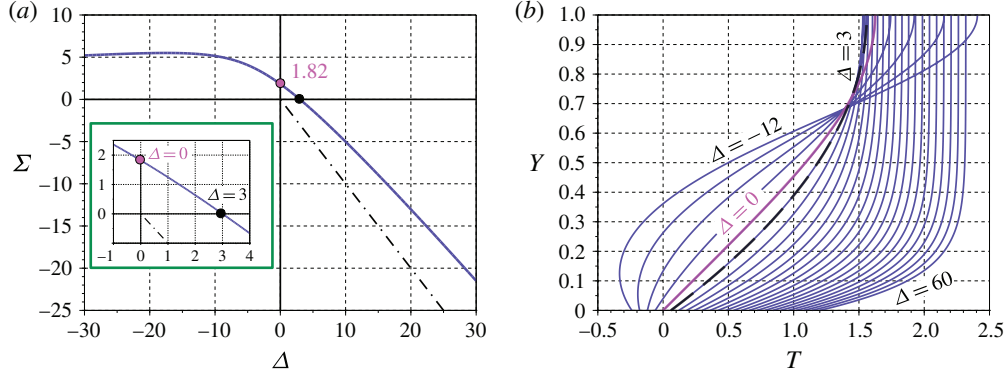


FIGURE 2. (a) Branch of solutions $\Sigma = \mathcal{S}(\Delta)$ for $\Delta \in [-30, 30]$ and (b) corresponding profiles $T_\Delta(Y) + \Delta/50$ (the shift is for clarity) for $\Delta \in [-12, 60]$. The special value $\mathcal{S}(0) \sim 1.82$ is shown in magenta.

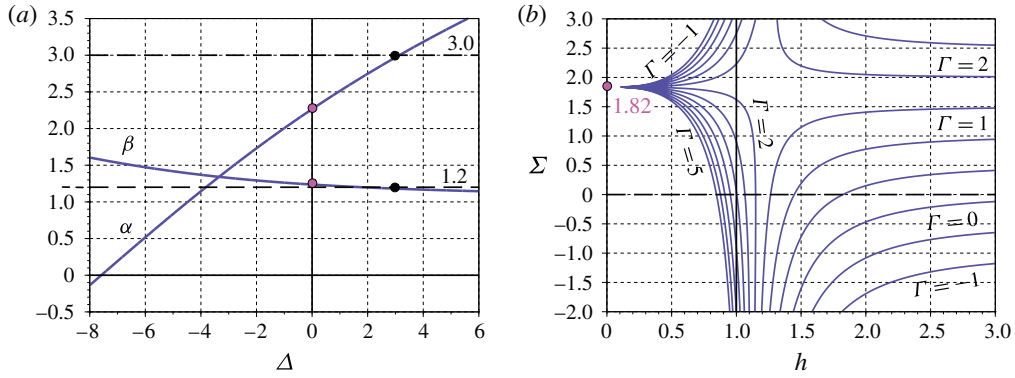


FIGURE 3. (a) Plot of $\alpha(\Delta)$ and $\beta(\Delta)$. (b) Slope $\Sigma = h_X$ as a function of h for $\Gamma \in [-1, 5]$.

2.3. Determination of the transcritical point with the NOR and STL models

We denote by NOR the model for which $\alpha = 3$ and $\beta = 1.2$ are kept constant, as if the velocity profiles were stuck to the parabola of the normal flow that would be obtained for $h = h_n = (3/\Gamma)^{1/3}$. The backwater curves are thus solutions of the ordinary differential equation $h'(X) = [h^3 \Gamma(X) - 3](h^3 - 1.2)^{-1}$. The general solutions of the NOR model can be sought by considering the family of trajectories $[X(s), h(s)]$ that are solutions of the system $\dot{X} = D(h)$ and $\dot{h} = N(X, h)$ with $D(h) = h^3 - 1.2$ and $N(X, h) = h^3 \Gamma(X) - 3$. The critical point (X_c, h_c) , forming a saddle node for the phase portrait of the dynamical system, is obtained for $D(h_c) = N(X_c, h_c) = 0$, leading to $h_c = 1.2^{1/3}$ and $\Gamma_c(X_c) = \Gamma_c = 2.5$. The linearization of the dynamical system around the critical point leads to the matrix \mathbf{A} with the components $A_{11} = 0$, $A_{12} = D'(h_c) = 3h_c^2$, $A_{21} = h_c^3 \xi$ and $A_{22} = 3h_c^2 \Gamma_c$ where $\xi = \Gamma'(X_c)$ measures the curvature of the bottom at the critical point. The ‘eigenslopes’ of \mathbf{A} , that is the slope of its eigenvectors, read

$$\Sigma_{\pm}(\xi) = \frac{\Gamma_c}{2} \left(1 \pm \sqrt{1 + \frac{4\xi h_c}{3\Gamma_c^2}} \right). \quad (2.7)$$

It appears that this expression is also valid for the STL model (2.6) with $h_c = 1$ and $\Gamma_c = 3$. To prove it, we consider, as for the NOR model, the following dynamical system:

$$\left. \begin{aligned} \dot{X} &= D[X, h, \dot{h}/\dot{X}] \quad \text{with } D(X, h, \Sigma) = h^3 - \beta(h^3[\Gamma(X) - \Sigma]), \\ \dot{h} &= N[X, h, \dot{h}/\dot{X}] \quad \text{with } N(X, h, \Sigma) = h^3 \Gamma(X) - \alpha(h^3[\Gamma(X) - \Sigma]). \end{aligned} \right\} \quad (2.8)$$

At first, the critical point is at the intersection of the lines $\dot{h} = 0$ and $\dot{X} = 0$ in the (X, h) plane. The first condition reads $\Delta = \alpha(\Delta)$, leading to $\Delta = 3$ and $h = h_n(X) = [3/\Gamma(X)]^{1/3}$. It describes the lines of the normal heights as $\Sigma = 0$. The second condition can be satisfied only when $h'(X) \rightarrow -\infty$ and leads to $h = 1$ since it can be numerically checked that $(1 - \beta)/\alpha \rightarrow 0$ when $\Delta \rightarrow +\infty$. As announced, we find $h_c = 1$ and $\Gamma(X_c) = 3$ when both conditions are met.

We now determine whether a straight line trajectory with the equation $X_\Sigma(s) = X_c + \eta(s)$ and $h_\Sigma(s) = h_c + \Sigma\eta(s)$, where Σ is a constant and $\eta(s) = \exp(\lambda s)$ is a small parameter, can satisfy (2.8) at the dominant order of $\eta \ll 1$. Such a property is equivalent to

$$\left. \begin{aligned} \mathbf{L}(\Sigma) \cdot \phi &= \lambda \phi \quad \text{with } \phi = \begin{pmatrix} 1 \\ \Sigma \end{pmatrix}, \quad \mathbf{L}(\Sigma) = \mathbf{A} + \mathbf{B}(\Sigma), \\ \mathbf{A} &= \begin{pmatrix} 0 & 3h_c^2 \\ h_c^3 \xi & 3h_c^2 \Gamma_c \end{pmatrix} \quad \text{and} \quad \mathbf{B}(\Sigma) = \begin{pmatrix} -h_c^3 \xi \beta' & -3h_c^2 (\Gamma_c - \Sigma) \beta' \\ -h_c^3 \xi \alpha' & -3h_c^2 (\Gamma_c - \Sigma) \alpha' \end{pmatrix}, \end{aligned} \right\} \quad (2.9)$$

where $\xi = \Gamma'(X_c)$, $\alpha' = \alpha'[h_c^3(\Gamma_c - \Sigma)]$ and $\beta' = \beta'[h_c^3(\Gamma_c - \Sigma)]$. We have $\mathbf{A} \cdot \phi = \lambda \phi$ under the conditions $\lambda = 3h_c^2 \Sigma$ and $h_c^3 \xi + 3h_c^2 \Gamma_c \Sigma = 3h_c^2 \Sigma^2$. In that case, we see that $\mathbf{B}(\Sigma) \cdot \phi = \mathbf{0}$. This shows that if Σ is a critical slope of \mathbf{A} , it is also a critical slope of $\mathbf{L}(\Sigma)$ while being given by (2.7). We note that this property is independent of the functions $\alpha(\Delta)$ and $\beta(\Delta)$, whose roles are confined to the determination of h_c and Γ_c .

3. Numerical simulations of critical transitions over obstacles

3.1. Numerical method for the TLM model and constant slope comparison

In order to solve (2.5) numerically, we discretize the variables X and h into successive values X^i and h^i for $i = 1, \dots, H$. Choosing two positive weights θ and ζ such that $\theta + \zeta = 1$, we build an implicit finite difference scheme to solve for the system (2.5) in the form

$$\begin{aligned} 0 &= (\theta T_{YY}^{i-1} + \zeta T_{YY}^i) + (h^{i-1} + \zeta dh^i)^3 (\Gamma - \Sigma) + \Sigma [\theta (T^{i-1})^2 + \zeta (T^i)^2] \\ &\quad + \frac{h^{i-1} + \zeta dh^i}{dh^i} \Sigma [(M^i - M^{i-1})(\theta T_Y^{i-1} + \zeta T_Y^i) - (T^i - T^{i-1})(\theta T^{i-1} + \zeta T^i)], \end{aligned} \quad (3.1)$$

where the bottom slope is $\Gamma = \theta \Gamma(h^{i-1}) + \zeta \Gamma(h^i)$. The surface slope Σ that results from this implicit equation must be considered as $\Sigma = \theta \Sigma^{i-1} + \zeta \Sigma^i$. As $dh^i = h^i - h^{i-1}$, we then set $dh^i = \Sigma dX^i$ with $dX^i = X^i - X^{i-1}$ to simulate the differential equation $h_X = \Sigma$ with an explicit Euler scheme. These steps are modified near singularities. The vertical scheme is the same as the one used for the STL model. We denote by $T^0(Y) = T_0(Y)$ the initial condition. A centred scheme $\theta = \zeta = 1/2$ has been chosen.

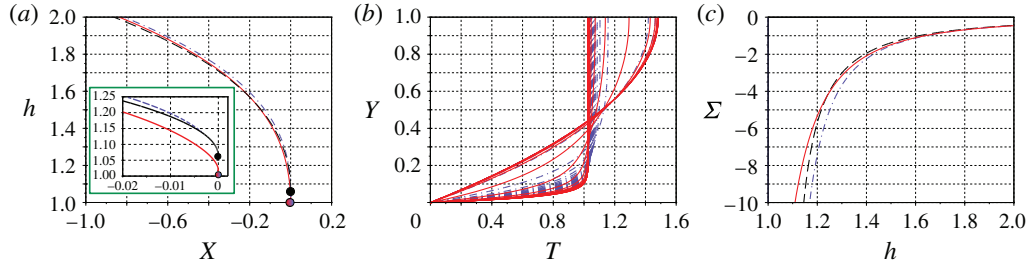


FIGURE 4. Comparison of the TLM (plain red), STL (dash-dotted blue) and NOR (dashed black) models near a surface slope singularity at $X = 0$ for $\Gamma = 0$. (a) Backwater curve $h(X)$. (b) Associated velocity profiles $T(X)$. (c) Corresponding curves $\Sigma = h'(X)$ as functions of h .

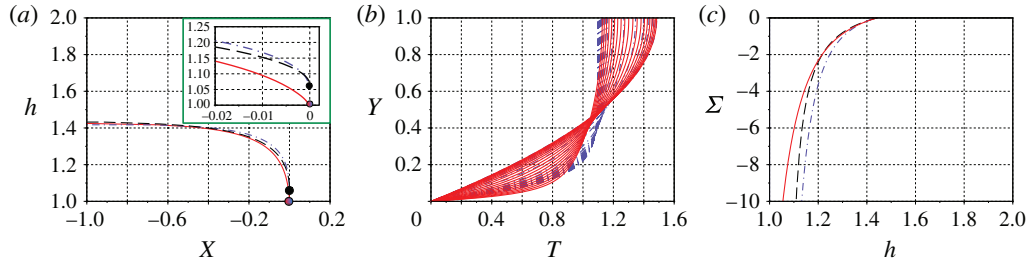


FIGURE 5. Same as figure 4 for $\Gamma = 1$. In contrast to the $\Gamma = 0$ case, $h_n \sim 1.44$ is bounded.

A first comparison between the TLM, STL and NOR models is made for the case of constant slope $\Gamma = 0$. We start with an initial condition with h_0 high enough that $T_0(Y)$ can be approximated by a parabola. A singularity at finite length is expected as shown in figure 4. The singularities of the three models have been translated to $X = 0$ in order to compare them. The heights of these backwater curves differ by only 5%, which is also the order of magnitude of the difference between the critical height $h_c = 1$ of the TLM and STL models and the critical height $h_c \sim 1.06$ of the NOR model. Similar results are found with non-vanishing slopes $\Gamma \neq 0$ (e.g. figure 5). These flows can be viewed as the fluvial regime of a transcritical transition through a bottom slope discontinuity.

3.2. Phase portraits for semi-parabolic bottom shapes

We now choose a semi-parabolic bottom profile $Z_f(X)$ such that $\Gamma(X) = -Z'_f(X)$ reads $\Gamma(X) = \xi X$ for $X \geq 0$ and $\Gamma(X) = 0$ for $X \leq 0$. A comparison of the phase portrait for the TLM, STL and NOR models is shown in figure 6 for two values of ξ . The initial conditions, taken at $X = -1$, are set to explore the vicinity of the TLM critical point reached for $X = 3$ for $\xi = 1$ and $X = 0.3$ for $\xi = 10$. The initial velocity profile for the TLM is computed from the STL model for the same value of initial height h_0 . A fine tuning of these values (up to twelve digits) shows that $(\Gamma_c, h_c) \sim (3, 1)$ as predicted by our theory.

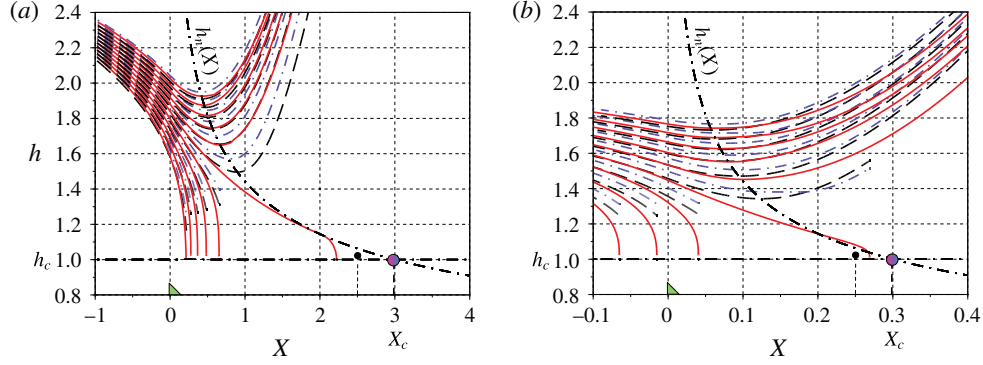


FIGURE 6. Phase portrait comparison between the TLM (plain red), the STL (dash-dotted blue) and the NOR (dashed black) models for a parabolic bottom ramp $Z_f(X) = -\xi X^2/2$ for $X \geq 0$ and $Z_f(X) = 0$ for $X \leq 0$. The normal heights $h_n(X)$, defined for $X > 0$, are shown by dashed-dotted lines. Determination of the critical point for (a) $\xi = 1$ and (b) $\xi = 10$.

The negative slope of the critical trajectory in the (X, h) plane can be compared to the expression (2.7) that reads here

$$\Sigma_-(\xi) = \frac{3}{2} \left(1 - \sqrt{1 + \frac{4\xi}{27}} \right) = -\frac{1}{9}\xi + \frac{1}{243}\xi^2 + O(\xi^3). \quad (3.2)$$

This can be done visually by considering the curve of the normal height profiles $h_n(X) = [\Gamma(X)/3]^{1/3}$ and noticing that $h'_n(X_c) = -\xi/9$. For $\xi = 1$, the proximity of the slopes $\Sigma_-(1) \sim h'_n(X_c) \sim -0.11$ can be seen in figure 6. For $\xi = 10$, the discrepancy between $\Sigma_-(10) = -0.86$ and $h'_n(X_c) = -1.11$ can be discerned visually.

These backwater phase portraits help to explain why the NOR model fails to catch the correct values of Γ_c and h_c . Indeed, the singularities of the phase portraits are associated with plug-like velocity profiles $T(Y)$ with $\beta = \int_0^1 T^2 dY \rightarrow 1$ while this shape factor is stuck at $\beta = 1.2$ for the NOR model.

3.3. Bottom shape inverse problem and validation of the critical slope relation

Rather than computing the unique critical backwater $h(X)$ that links the fluvial and torrential regimes for a given bottom slope profile $\Gamma(X)$, which is cumbersome, we consider the inverse problem of computing the latter, given the former. This is done by considering that Σ and Γ are respectively known and unknown in the implicit (3.1).

We choose $h(X) = \bar{h} + \Delta h \tanh(X/L)$ with $\bar{h} = (h_1 + h_2)/2$ and $\Delta h = (h_2 - h_1)/2$ such that $h_1 = (3/\Gamma_1)^{1/3}$ and $h_2 = (3/\Gamma_2)^{1/3}$ are the normal heights associated with the bottom slopes $\Gamma_2 > \Gamma_1$. The corresponding $\Gamma(X)$ in the cases $\Gamma_1 = 1$, $\Gamma_2 = 4$ and $L = 0.8$ is displayed in figure 7(a) for both the TLM and STL models. Further numerical experiments show that the discrepancy between the two models disappears when L increases. We also observe that $\Gamma \sim 3$ when $h = 1$, which confirms the value of the critical slope $\Gamma_c = 3$. This defines the location X_c of the critical point. For each value of L , we then compute $\xi = \Gamma'(X_c)$, which traces back the curvature of the bottom at the critical point. Its relation with the critical slope $\Sigma_c = \Sigma(X_c)$ is shown in figure 7(b) and compared (dashed-dotted blue curve) with the function $\Sigma_-(\xi)$ of (3.2), derived from the STL model. We observe a satisfactory agreement compared to

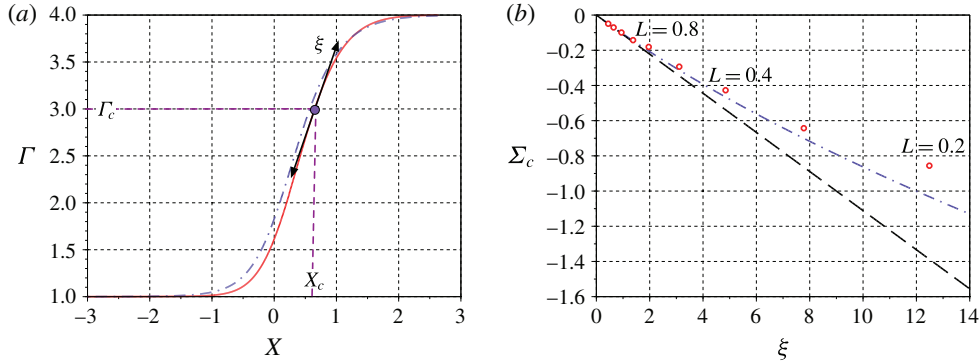


FIGURE 7. Slope $\Gamma(X)$ such that $h(X) = \bar{h} + \Delta h \tanh(X/L)$ is the critical backwater curve in the cases $\Gamma_1 = 1$ and $\Gamma_2 = 4$. (a) Comparison between the TLM (plain red) and the STL (dash-dotted blue) for $L = 0.8$. (b) Critical surface slope $\Sigma_c = h'(X_c)$ as a function of the bottom curvature $\xi = \Gamma'(X_c)$ for $L = 2^{k/2}/10$ and $k = 2, 3, \dots, 11$. Comparison with the theoretical functions for the STL (dash-dotted blue) and the NOR (dashed black) models.

the NOR model, which can only predict a critical slope $\Sigma_c = h'_n(X) = -\xi/9$ given by the normal height profile $h_n(X)$.

4. Conclusion

We have shown that the STL model, based on a similarity assumption $u = T(y/h)/h$ for the streamwise velocity $u(X, y)$, could provide a reasonable approximation of the TLM model that takes into account the X -dependency of $u = T(X, y/h)/h$ beyond that of the height profile $h(X)$. We proved this to be the case for the critical transition of a laminar shallow-water flow in the presence of a bottom with increasing slope $\Gamma(X)$. Through numerical simulations of the TLM model, which involve the resolution of an implicit nonlinear differential equation, we have checked the validity of the relation (3.2) between the critical surface slope $\Sigma_c = h'(X_c)$ and the bottom curvature factor $\xi = \Gamma'(X_c)$ computed at the critical location $X = X_c$.

We have shown that the critical values were $h_c = 1$ and $\Gamma_c = 3$ for a Newtonian rheology in the laminar case, contrarily to the commonly used NOR model that leads to $h_c = 1.2^{1/3} \sim 1.06$ and $\Gamma_c = 2.5$, as shown in § 2.3. Other rheologies would provide different values in the framework of the STL approach. Indeed, these generalizations lead to different functions $\alpha(\Delta) = T'(0)$, related to the bottom friction, and $\beta(\Delta) = \int_0^1 T^2 dY$, related to the shape of the velocity profiles. These functions provide the values of $h_c^3 = \lim_{\Delta \rightarrow \infty} \beta(\Delta)$ and Γ_c as the solution of $\Delta_n = \alpha(\Delta_n)$ with $\Delta_n = h_c^3 \Gamma_c$. But there is a universality of the critical slope expression through (2.7) that involves only h_c , Γ_c and $\xi = \Gamma'(X_c)$.

The STL model is likely to provide a good approximation of the TLM model for other shallow-water regimes, as is suggested by comparison of the backwater curves of the two models, for instance in the (h, Σ) representation of figure 3. Such an exhaustive plot in the case of the TLM model could not be shown here due to numerical problems that lead to instabilities or failure of the implicit problem resolution for some regions of the (h, Σ) plane. Numerical methods to overcome this difficulty are to be explored. This could validate the complex classification of the backwater curves associated with the STL model, due to multiple values of $\Sigma = h'(X)$ as a function of h for $\Gamma \in [1.82, 3]$.

An extension of our approach to unsteady flows is under way. This could improve the temporal and spatial stability analysis of the normal flows (Thual, Plumerault & Astruc 2010, and references therein). We think that numerous flow analyses, such as roll waves or hydraulic jumps (Thual 2013, and references therein), could be enriched in the light of these TLM and STL shallow-water models. Their generalization to non-Newtonian rheologies and turbulence parameterization is possible. Finally, taking into account capillarity effects in these models is worth pursuing in order to address, with our approach, the vast literature devoted to thin viscous films.

Acknowledgement

This work was performed in the framework of the PHYSCALE project of the RTRA STAE foundation (<http://www.fondation-stae.net>).

References

- ALEKSEENKO, S. V., NAKORYAKOV, V. YE. & POKUSAEV, B. G. 1985 Wave formation on a vertical falling liquid film. *AIChE J.* **31** (9), 1446–1460.
- BENNEY, D. J. 1966 Long waves on liquid films. *J. Math. Phys.* **45** (2), 50–155.
- BOUTOUNET, M., CHUPIN, L., NOBLE, P. & VILA, J.-P. 2008 Shallow water viscous flows for arbitrary topography. *Commun. Math. Sci.* **6** (1), 29–55.
- BUKREEV, V. I., GUSEV, A. V. & LYAPIDEVSKII, V. YU. 2002 Transcritical flow over a ramp in an open channel. *Fluid Dyn.* **37** (6), 896–902.
- CHAKRABORTY, S., NGUYEN, P.-K., RUYER-QUIL, C. & BONTOZOGLOU, V. 2014 Extreme solitary waves on falling liquid films. *J. Fluid Mech.* **745**, 564–591.
- CHOW, V. T. 1959 *Open-channel Hydraulics*. McGraw-Hill.
- FERNÁNDEZ-NIETO, E. D., NOBLE, P. & VILA, J.-P. 2010 Shallow water equations for non-newtonian fluids. *J. Non-Newtonian Fluid Mech.* **165** (1314), 712–732.
- GJEVIK, B. 1970 Occurrence of finite amplitude surface waves on falling liquid films. *Phys. Fluids* **13** (8), 1918–1925.
- KAPITSA, P. L. & KAPITSA, S. P. 1949 Wave flow of thin layers of a viscous liquid. *Zh. Eksp. Teor. Fiz.* **19**, 105–120.
- LIN, S. P. 1969 Finite-amplitude stability of a parallel flow with a free surface. *J. Fluid Mech.* **36**, 113–126.
- NAKAYA, C. 1975 Long waves on a thin fluid layer flowing down an inclined plane. *Phys. Fluids* **18** (11), 1407–1412.
- NGUYEN, L. T. & BALAKOTAIAH, V. 2000 Modeling and experimental studies of wave evolution on free falling viscous films. *Phys. Fluids* **12** (9), 2236–2256.
- NOBLE, P. & VILA, J.-P. 2013 Thin power-law film flow down an inclined plane: consistent shallow-water models and stability under large-scale perturbations. *J. Fluid Mech.* **735**, 29–60.
- ORON, A., DAVIS, S. H. & BANKOFF, S. G. 1997 Long-scale evolution of thin liquid films. *Rev. Mod. Phys.* **69**, 931–980.
- PUMIR, A., MANNEVILLE, P. & POMEAU, Y. 1983 On solitary waves running down an inclined plane. *J. Fluid Mech.* **135**, 27–50.
- ROBERTS, A.J. 1996 Low-dimensional models of thin film fluid dynamics. *Phys. Lett. A* **212** (12), 63–71.
- RUYER-QUIL, C. & MANNEVILLE, P. 1998 Modeling film flows down inclined planes. *Eur. Phys. J. B* **6** (2), 277–292.
- RUYER-QUIL, C. & MANNEVILLE, P. 2000 Improved modeling of flows down inclined planes. *Eur. Phys. J. B* **15** (2), 357–369.
- RUYER-QUIL, C. & MANNEVILLE, P. 2005 On the speed of solitary waves running down a vertical wall. *J. Fluid Mech.* **531**, 181–190.
- SADIQ, I. M. R. & USHA, R. 2008 Thin newtonian film flow down a porous inclined plane: stability analysis. *Phys. Fluids* **20** (2), 022105.

- DE SAINT-VENANT, B. 1871 Théorie du mouvement non permanent des eaux, avec application aux crues des rivières et à l'introduction des marées dans leur lit. *C. R. Acad. Sci. Paris* **73**, 147–154.
- SAMANTA, A., RUYER-QUIL, C. & GOYEAU, B. 2011 A falling film down a slippery inclined plane. *J. Fluid Mech.* **684**, 353–383.
- SCHLICHTING, H. 1955 *Boundary-layer Theory*. McGraw-Hill.
- SCILAB ENTERPRISES 2012 *Scilab: Free and Open Source Software for Numerical Computation*, Scilab Enterprises, (<http://www.scilab.org>).
- SERRE, F. 1953 Contribution à l'étude des écoulements permanents et variables dans les canaux (Contribution to the study of steady and unsteady channel flows). *La Houille Blanche* **8**, 830–887.
- SHKADOV, V. Y. 1967 Wave flow regimes of a thin layer of viscous fluid subject to gravity. *Fluid Dyn.* **2** (1), 29–34.
- SHKADOV, V. Y. & SISOEV, G. M. 2004 Waves induced by instability in falling films of finite thickness. *Fluid Dyn. Res.* **35** (5), 357–389.
- THUAL, O. 2013 Modelling rollers for shallow water flows. *J. Fluid Mech.* **728**, 1–4.
- THUAL, O., PLUMERAULT, L.-R. & ASTRUC, D. 2010 Linear stability of the 1d Saint-Venant equations and drag parameterizations. *J. Hydraul Res.* **48** (3), 348–353.
- ZERIHUN, Y. T. & FENTON, J. D. 2006 One-dimensional simulation model for steady transcritical free surface flows at short length transitions. *Adv. Water Resour.* **29** (11), 1598–1607.